ACS APPLIED NANO MATERIALS

www.acsanm.org Article

Anisotropically Functionalized Nanotube Anchors for Improving the Mechanical Strength of Immiscible Polymer Composites

Lawrence Barrett, Fatoumata Ide Seyni, Mallikharjuna Rao Komarneni, John A. Zapata-Hincapie, Daniel T. Glatzhofer, Brian P. Grady, and Steven Crossley*

Cite This: *ACS Appl. Nano Mater.* 2021, 4, 580–589 Read Online

ACCESS | Metrics & More | Article Recommendations | Supporting Information

ABSTRACT: Plastic recycling is limited due to the immiscibility of most polymers and the weakness of the corresponding interface. Here, a method to synthesize block nanotubes in a scalable manner is described, and one example is shown where these nanotubes strengthen polymer−polymer interfaces. The method relies on the incorporation of nitrogen atoms selectively within the nanotube structure during growth. By rapidly changing the reaction environment, blocks of nitrogen functionality along the length of the nanotube result. The change in the local electronic environment and radical scavenging property of the nanotube near the nitrogen atoms was used to selectively polymerize styrene from the nanotube wall where nitrogen is incorporated. These diblock-functionalized nanotubes were placed at a poly(methyl methacrylate)/polystyrene (PMMA/PS) interface, and the fracture toughness was measured by the asymmetrical double cantilever beam test. The fracture toughness of the interface was found to increase by over 1000% compared to that of the bare interface and 400% over the interface with nonfunctionalized nanotubes.

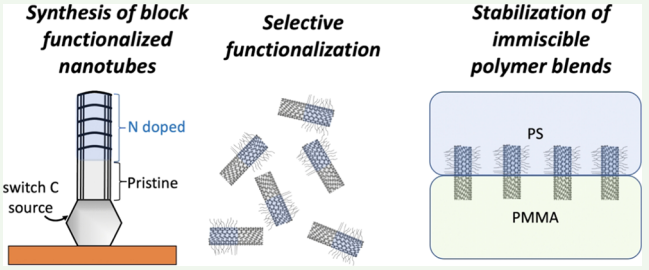

KEYWORDS: *nanotubes, polymer recycling, plastics, polymer−polymer interface, nitrogen-doped*

INTRODUCTION

Over the past few decades, there has been a definitive trend of increasing plastics recycling although overall recycling rates in the United States are less than 10% as of 2015.[1] One primary reason for the low recycle rates is the fact that most polymers are immiscible with one another, which means that mechanical properties of polymer blends are far less than that of the individual components because of very weak interfaces between two immiscible polymers.[2−4] Hence, essentially all mechanical recycling processes involving postconsumer materials have a separation step as part of the process, so that polymers of one type are segregated from one another. Further, the proliferation of multilayer films, especially in food packaging, has meant that segregation by type is not possible for some products.

A well-studied and often-used strategy to strengthen interfacial adhesion in polymer−polymer blends is via the introduction of diblock copolymers where the blocks are chosen to match the two polymers. Unfortunately, however, diblock copolymers will occasionally aggregate in one of the polymer phases instead of migrating to the interface.[2−4] Micellar aggregates are entropically favorable when compared to dispersion of a copolymer at the interface, and once formed, they are difficult to break. Tetrablock and higher copolymers will not form micelles and have been proven to strengthen the blend interface[5,6] but will form lamellar layers under shear stress.[6] Schmalz et al. have developed a method to use the micelle formation of block copolymers to create "patchy" polymer-coated carbon nanotubes (CNTs).[7,8] A polystyrene (PS)/polyethylene (PE)/poly(methyl methacrylate) (PMMA) triblock polymer was physically wrapped around the nanotube using the strong interactions of polyethylene with the nanotube to bind it in place. The nonanchoring groups, PS and PMMA, then formed micelles around the nanotube resulting in patches of polymer on the surface and a nanotube that is block-functionalized in the radial direction. These polymer-coated nanotubes were dispersed in a PMMA/PS blend and had a strong influence on the domain area of the PMMA phase, possibly indicating a strengthening of the interface although no quantitative data was shown. Transmission electron microscopy (TEM) shows the nanotubes laying at and parallel to the blend interface. Carbon nanotubes are remarkably strong along the axial direction[9,10] but are much weaker radially,[11−13] meaning if the nanotube lays along the blend interface and not perpendicular to the interface, then the full strengthening potential of the nanotube is not used. Further, when the polymer is not chemically bound to the

Received: October 28, 2020
Accepted: November 20, 2020
Published: December 19, 2020

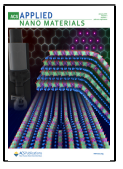

https://dx.doi.org/10.1021/acsanm.0c02886
ACS Appl. Nano Mater. 2021, 4, 580−589

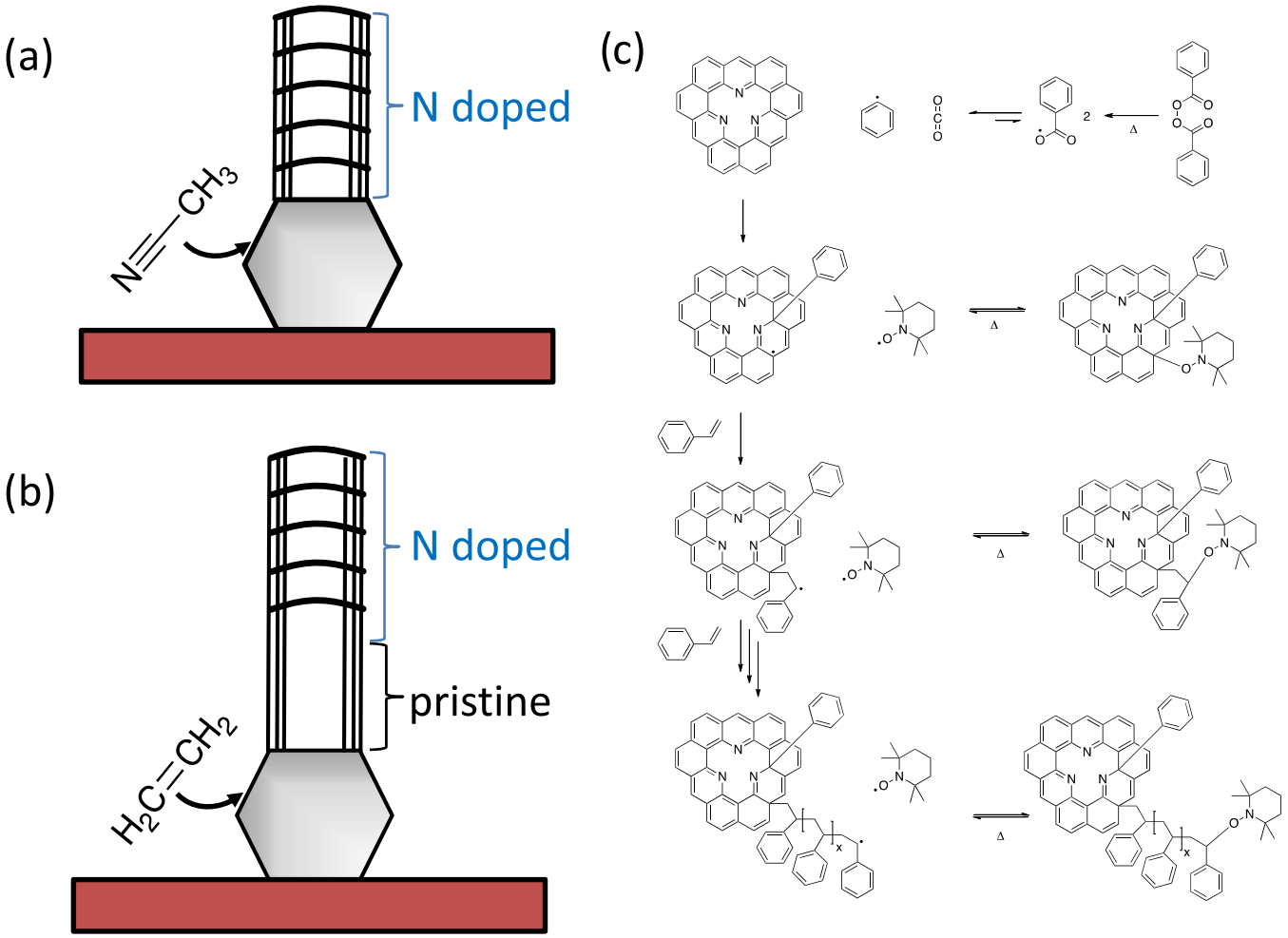

Figure 1. Schematic depiction of sequential (a) N-doped nanotube growth followed by (b) nondoped carbon nanotube growth. (c) Radical growth of polymer on nitrogen-modified carbon nanotubes.

nanotube, depending on the conformation of the polymer chain around the nanotube, the weakest point in the system will be van der Waals forces between the nanotube and polymer, which is much weaker than a covalent bond. Another technique grafts a polymer and a reactive group along the length of a carbon nanotube, where the two are chosen so that the polymer prefers one component and the reactive group can only react with the other component. Micrographs indicate that the nanotubes are located at the interface, but their orientation does not appear normal to the interface. No direct measurement of interfacial strength is made, but the elongation at break and toughness increase by more than 20 times.[14] However, there are also significant changes in morphology, so it is unclear how much the change in morphology contributes to the performance vs a change in interfacial strength.

Previous work from our group[15] and others[16−19] has shown that CNTs with uniform surface chemistry will reside entirely within the phase most compatible with their surface functional groups. Producing nanotubes that will reside along an interface or cross through the interface to serve as an anchor can be accomplished by placing anisotropic blocks of functional groups along the length of the nanotube. While anisotropically functionalized, or block-functionalized carbon nanotubes (BF-CNTs) have been produced,[20−24] the selective multilayer masking and sample manipulation involved in this approach limit these materials to very small-scale (mg) applications. In this work, we will describe a new method for producing BF-CNTs in a scalable manner using wet chemistry and fluidized beds. This method can generate sample amounts appropriate to demonstrate their potential for stabilizing melts of immiscible polymer blends. The extent to which the BF-CNTs strengthen the interface is investigated. In addition to the stabilizing potential of carbon nanotubes, their excellent ability to conduct heat and electricity can enable a broad range of applications with highly tunable tensile strengths[25] if a block nanotube were controllably placed at the interface.

RESULTS AND DISCUSSION

Most nanotube functionalization approaches use strong oxidative or acidic conditions[26] that do not impart selectivity of functional groups along the length of the tube. As an alternative, functional groups have been incorporated during the growth process by the selective incorporation of nitrogen species. Nitrogen can be incorporated directly into the nanotube wall during growth[27,28] based on the feedstock and has been well studied in graphene and nanotubes.[27−31] In addition to incorporating nitrogen groups, we synthesized nanotubes between sheets of vermiculite within a fluidized bed to minimize cleavage of the nanotubes due to attrition during the growth. This approach enabled the uniform forest that is typical of vertically aligned nanotube growth and protection from physical damage while still in the scalable fluidized bed

https://dx.doi.org/10.1021/acsanm.0c02886
ACS Appl. Nano Mater. 2021, 4, 580−589

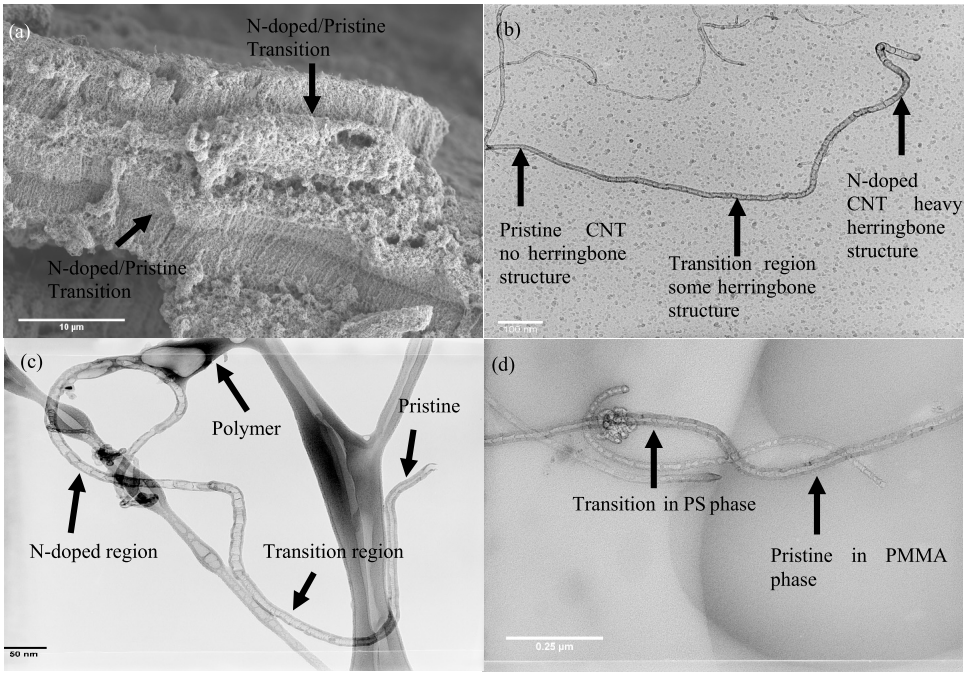

Figure 2. (a) SEM image of block CNTs on vermiculite, which shows a coloration difference in the two halves of the nanotube, perhaps indicating a difference in conductivity or amorphous carbon on the surface. (b) TEM image of block nanotubes, showing a nitrogen content gradient along the length, the left portion showing no nitrogen content, and the right portion has heavy herringbone structures indicating nitrogen heteroatoms, with a transition region in between. (c) TEM image of a block-grown nanotube after polymerization supported on a lacey carbon grid. Polymer is only found on the portion of the nanotube-containing herringbone structures. (d) TEM image of a BF-CNT at a PS/PMMA interface. The nanotube herringbone structure indicates where polymer would have been attached, near the nitrogen atoms.

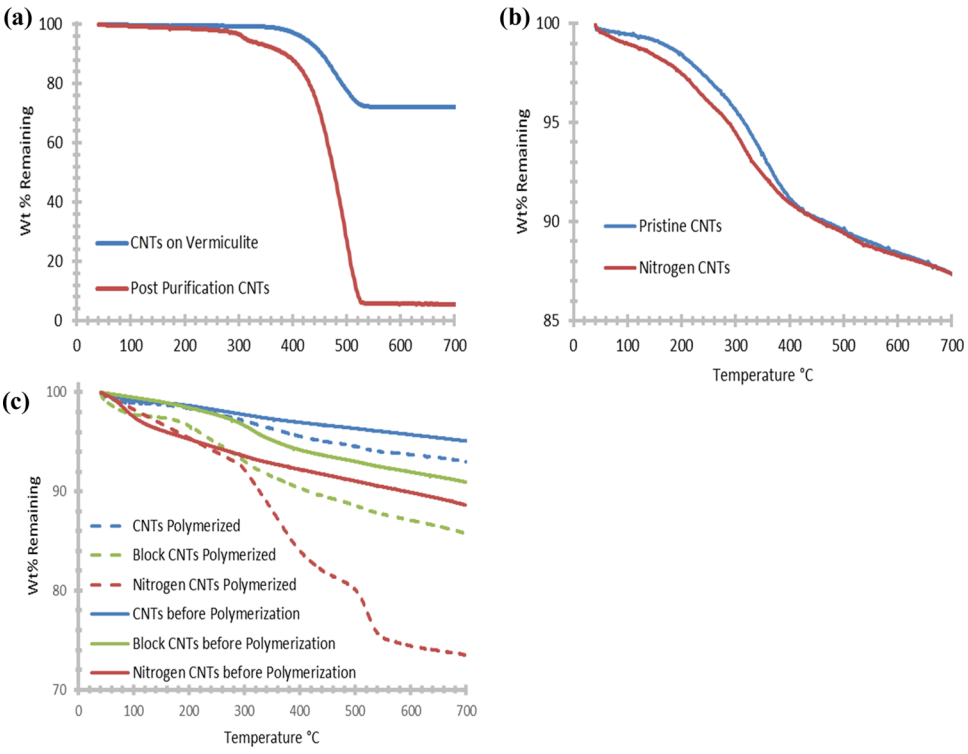

Figure 3. (a) Thermal decomposition of CNTS in air before and after purification. (b) Thermogravimetric analysis (TGA) graph of the radical initiator/mediator thermally leaving the surface in argon. (c) Thermal decomposition of the polymer/nanotube composite in argon.

reactor. The lamellar structure of vermiculite, consisting of alumina silicates and magnesium oxide,[32] was dissolved by treatment with a strong base[33] followed by a weak acid.[34] Any exposed catalyst particles will be removed with the acid wash. These treatments should not have affected the surface chemistry of the nanotube surface.[26,35]

After synthesis of block-functionalized nanotubes, polymer chains were attached selectively to the nitrogen-containing

https://dx.doi.org/10.1021/acsanm.0c02886
ACS Appl. Nano Mater. 2021, 4, 580−589

walls via a "grafting-from" method, as illustrated in Figure 1. For simplicity, and to reflect steric interaction with the added phenyl ring, combination with the 2,2,6,6-tetramethyl-1-piperidinyloxy (TEMPO), and addition to styrene, is depicted here as occurring at the carbon allylic to the N and to the site of phenyl radical addition. Pyridine rings are shown clustered in groups of three because a single nitrogen functionality leaves dangling carbon bonds or results in a graphitic nitrogen. Graphitic nitrogen does occur but is likely to be restricted to the inner walls of multiwalled nanotubes due to diffusion limitations during synthesis.[36]

The nitrogen in the nanotube's outer walls is primarily incorporated in the form of pyridine rings,[27,28,30] which are more reactive than benzene-type rings. Terrones et al.[37] have used this reactivity along with the radical scavenging tendencies of CNTs to create a semi-stable resonant radical structure on the addition of benzoyl peroxide radicals to nitrogen-containing CNTs, CN_xNT. Using benzoyl peroxide as the radical source will result mainly in the addition of phenyl radicals to the nanotubes, and addition will most likely occur at the 2-position adjacent to the N atom.[38,39] Some addition of benzyloxy radicals likely takes place, and the addition of radicals may take place at other positions as well but is not depicted in Figure 1 for clarity. This resonant radical structure can combine with 2,2,6,6-tetramethyl-1-piperidinyloxy, TEMPO, as a mediator to perform nitroxide-mediated radical polymerization, NMRP, to grow polystyrene brushes on the surface of the CN_xNTs. The resulting radical on the nanotube will be delocalized, and combination with the TEMPO radical and polymer growth may occur at many positions but will become localized once polymerization starts. Since the reaction is occurring on a closed surface, both radical addition and reaction with TEMPO or styrene will likely take place on the *exo*-face of the outer nanotube. Other research groups have accomplished a similar feat on pristine CNTs without nitrogen functional groups,[40,41] but in these cases, oxidation of the nanotubes, 5 and 8 wt % carboxylic groups, respectively, was required to form polymerization sites. Terrones et al.[37] used nanotubes with 1 wt % N and 2.5 wt % O. Thermal gravimetric mass spectrometry (TG-MS) showed that the CN_xNT had a nitrogen content of 0.68 wt % and an oxygen content of 1.16 wt %.

Block nitrogen-containing nanotubes were grown on vermiculite-supported catalyst as shown in the scanning electron microscope (SEM) image of Figure 2a. A clear distinction between the two phases of the nanotube can be observed in the image. The lamellar layers of the vermiculite are composed of an alumina silicate and magnesium oxide. Figure 3a shows the thermal degradation of the block-functionalized nanotubes in air before and after purification, indicating that nearly all of the catalyst particles and vermiculite support have been removed. This is the first report of such purification of nanotubes on a vermiculite support.

TEM images performed on the block CN_xNTs demonstrate the presence of a concentration gradient of nitrogen in the nanotube. CN_xNTs grown with acetonitrile on an iron catalyst are well documented to exhibit a herringbone structure. Figure 2b shows a gradient of these herringbone structures from none on the left to a high concentration on the right, indicating that there is a gradient of nitrogen incorporated into the nanotube. Furthermore, while the length of the nanotube indicates that dispersion on the TEM grid by sonication caused some breakage, the breakage did not obviously occur at the nitrogen/pristine interface of the nanotube. Sonication is only used for dispersion on TEM grids, not for the purification and functionalization of the nanotubes. SEM of the functionalized nanotubes showed no significant breakage, as shown in the Supporting Information.

To evaluate the ability to create the resonant radical structures on the nanotube surface for subsequent polymerization, pure pristine and pure nitrogen-doped nanotubes were tested separately with the polymerization initiator and mediator. Nanotubes were reacted with the benzoyl peroxide initiator and TEMPO mediator and analyzed by TGA in argon to determine the number and stability of radical groups on the surface. As can be seen in Figure 3b, while the total amount of weight loss across the two samples is comparable, there is a clear difference in the temperature the radicals leave the surface, indicating that the nitrogen-doped nanotubes bind the radicals less strongly, perhaps by creating the resonant structures theorized by Terrones.[37] Therefore, pristine CNTs that bind the radicals more strongly are unable to release the mediator TEMPO for polymerization at low temperatures in agreement with the idea that surface groups can significantly modify the radical scavenging properties of nanotubes.[42,43]

Once the selectivity of radical groups on the surface was established, the nanotubes were dispersed in benzene and styrene and heated to 80 °C for polymerization to occur. Again, the pure pristine and pure CN_xNTs were tested first and underwent TGA in argon to determine the extent of polymerization. The results can be seen in Figure 3c, indicating more pronounced polymerization on nitrogen-doped nanotubes. Unpolymerized samples are also shown for comparison. The differences in low-temperature weight loss for the N-doped vs pristine nanotubes before polymerization can be attributed to differing degrees of moisture adsorption due to exposed nitrogen-containing functional groups.

Polymer chain lengths are challenging to measure while tethered to the nanotube surface, as molecular weights may decrease during the process of removal from the nanotubes. An estimate may be made by dividing the polystyrene desorbed from the nanotube surface via TGA measurements by the moles of TEMPO that has been thermally desorbed at 80 °C, the polymerization temperature. This approximation suggests an average polymer molecular weight of slightly over 3000 g/mol. Based on weight percentage, the selectivity for polymer growth over nitrogen-doped vs pristine nanotubes was about 7:1. The same functionalization procedure was performed on the block nitrogen-containing CNTs after accounting for moisture adsorption. Block tubes after polymerization were found to be 9.6 wt % polymer, which corresponds to having a 54% nitrogen doping assuming the same 7:1 ratio.

TEM was used to visually determine the polymer attachment to the block nanotube. Figure 2c shows block nanotubes after polymerization. A large amount of polymer can be seen in the upper portion of the nanotube, which contains herringbone structures, indicating that this is the portion of the nanotube-contained nitrogen heteroatoms. The pristine portion of the nanotube, however, showed no attached polymer. Of the hundreds of nanotubes observed, none showed polymer attached to the pristine surface, while 40% showed polymer on the nitrogen portion. TEM was also used to image nanotubes placed in a polymer blend, as can be seen in Figures 2d and S1. Figure 2d shows where the herringbone structure is located, which corresponds to the part functionalized with PS

https://dx.doi.org/10.1021/acsanm.0c02886
ACS Appl. Nano Mater. 2021, 4, 580−589

and is in the lighter PS phase, while the rest of the nanotube resides in the PMMA phase, which is darker. The nanotube bisects the interface at a nearly perpendicular angle, rather than having its length lay along the interface. As noted earlier, the stiffness and high aspect ratio of nanotubes will cause strong segregation of single-chemistry tubes into the preferred phase of interest; our observations here are consistent with that observation.

To further investigate the nature of selective polystyrene grafting to the nanotube surface, X-ray photoelectron spectroscopy (XPS) experiments were carried out on the nitrogen-doped samples pre- and post functionalization. Due to the surface-sensitive nature of the XPS technique, probing approximately three atomic layers deep within a solid surface, the measure of the surface alterations that occur upon polystyrene grafting is quite revealing. Peaks were deconvoluted based on identification of N-doped carbon structures reported by Biddinger et al.[44] Figure 4 illustrates that the N 1s

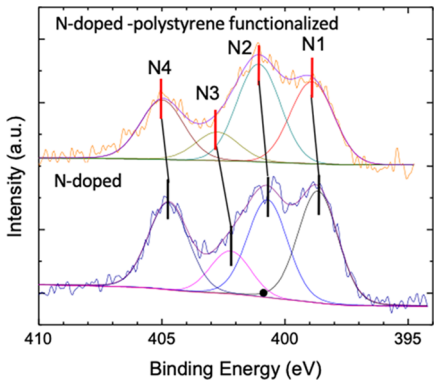

Figure 4. High-resolution XPS results for various fully nitrogen-doped nanotubes prior to and postpolystyrene polymerization. Deconvoluted peaks correspond to the species identified in Table 1.

spectrum obtained from the polystyrene-functionalized CNT sample shows the deconvoluted peaks at BEs of 398.91 eV (N1), 401.08 eV (N2), 402.75 eV (N3), and 404.99 eV (N4), as tabulated in Table 1. The observed positive shift in BEs (~0.25−0.5 eV) clearly indicates that polystyrene functionalization influences the surface chemistry of N-doped CNTs. Pyrrolic N is incorporated into five-membered heterocyclic rings and contributes two p electrons to the π system. This could be the reason for the slightly high positive BE shift (0.37 eV) of N2 peak when compared to that of pyridinic N (N1 peak shift of ~0.25 eV), which contributes only one p-electron to the aromatic π system. The pyridinic (N1), types of quaternary and graphitic (N3), and pyridinic oxide (N4) peak areas are reduced by ~25% each after polystyrene functionalization, with the only exception of pyrrolic (N2) peak that is slightly reduced (~3%). This distinction indicates that not all N species are covered to the same extent by PS grafting, further emphasizing the selective nature of said functionalization in the proximity of specific N surface features. There also has been a slight increase in the full width at half-maximum (FWHM) of N peaks of polystyrene-functionalized CNTs (2.07) when compared to that of the N-doped CNTs (1.91), corresponding to the adsorption of polystyrene, as shown in the Supporting Information. Table 2 shows the ratio of nitrogen to carbon

Table 2. Surface-Nitrogen-to-Carbon Ratios Obtained from XPS Analysis over Various Nanotube Samples before and after Polystyrene Growth

nanotube sample	nitrogen/carbon
pristine	
nitrogen (N)-doped	0.062
N-doped-polystyrene-functionalized	0.052
block	0.049
block-polystyrene-functionalized	0.033

obtained near the surface of these materials. Upon each incorporation of polystyrene, there is clearly a decrease in the N/C ratio, indicating that the N functional groups are selectively covered by polystyrene layers. It is intriguing that not all N functional groups are influenced, further illustrating the selective nature of grafting around specific surface features.

The effectiveness of these nanotubes at an immiscible polymer blend interface is probed by measurement of the fracture toughness, G_C, of the interface and is measured by the asymmetric double cantilever beam test, ADCB, as described by Creton.[45] TEM images of the block nanotubes at the prepared PS/PMMA interface for these tests are indicated in Figure 5. A cross section of these prepared interfaces was microtomed to 690 nm prior to imaging, with thinner slices leading to fracture at the interface and thicker slices not allowing sufficient light penetration for imaging. Of note only the block-functionalized nanotubes were readily imaged through this method, as both the bare interface and the interface laden with nanotubes containing a single chemistry fractured upon microtome slicing at this thickness, qualitatively indicating that the block-functionalized nanotubes are able to strengthen the interface. Of further note, as mentioned earlier, some aggregates of nanotubes are formed in the solution prior to spin coating, with these aggregates and entanglement apparent in Figure 5. This causes some nanotubes to lie at various orientations across the interface, although it is clear

Table 1. High-Resolution XPS Binding Energy Peak Shifts for Nitrogen-Doped Nanotubes Pre- and Postpolystyrene Polymerization

	sample	pyridinic	pyrrolic	types of quaternary	pyridinic oxide
binding energy (eV)	reference[a]	398.60	400.50	401.30	402−405
	N-doped	398.66	400.71	402.21	404.73
	N-doped-polystyrene-functionalized	398.91	401.08	402.75	404.99
peak shift (eV)		0.25	0.37	0.54	0.26
peak area (au)	N-doped	752	681	276	583
	N-doped-polystyrene-functionalized	571	658	208	434
decrease in peak area (%)		24	3	25	26

[a]Identifying various peaks from ref 44.

https://dx.doi.org/10.1021/acsanm.0c02886
ACS Appl. Nano Mater. 2021, 4, 580−589

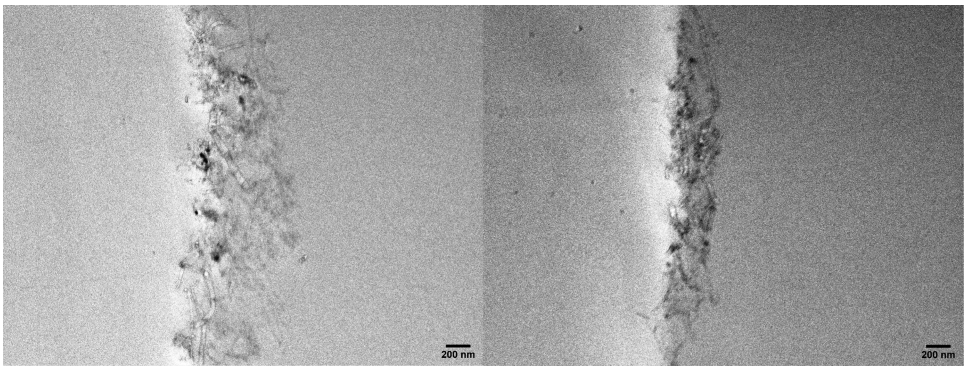

Figure 5. TEM images at two locations along the cross section of a PS/PMMA interface containing block-functionalized nanotubes after polystyrene polymerization. Nanotubes were deposited via solution casting prior to ADCB testing.

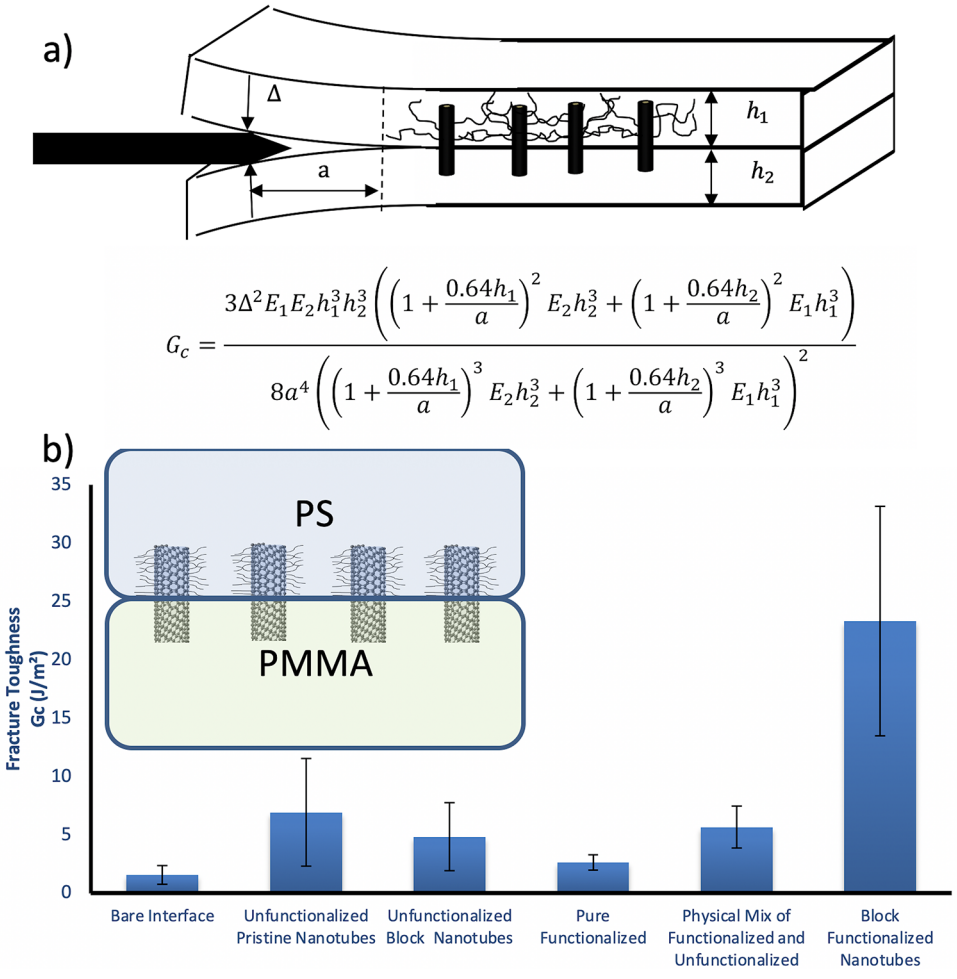

Figure 6. (a) Schematic of the asymmetric double cantilever beam test to measure fracture toughness. A razor blade is inserted slowly between two sheets of polymer that have been bound together. The length of the crack after propagation can be used with Young's moduli of the materials, E_i, height of the material, h_i, and the thickness of the razor, Δ, to calculate the fracture toughness. (b) Fracture toughness values determined by the asymmetrical double cantilever beam test for PS/PMMA wafers bound together with nanotubes deposited via spin coating as described in the methods section. Results are shown for pristine CNTs, block N-doped CNTS without polymer functionalization, pure N-doped CNTs with polymer functionalization, a 50/50 wt % physical mixture of the pristine CNTs and functionalized N-doped CNTS, and the block polymer-functionalized CNTS.

that some of the nanotubes do extend into both phases. This indicates that improved dispersion techniques to inhibit aggregation during block-functionalized nanotube preparation will likely improve any resulting effects on interfacial strengthening even further than what is indicated in the fracture toughness tests reported here.

A schematic of the ADCB testing apparatus can be seen in Figure 6a. Polystyrene and poly(methyl methacrylate) were used with a thickness ratio of 1.2:1 to account for the slightly different crazing stress as required by the test, and the results can be seen in Figure 6b. Pristine CNTs reside in the PMMA

https://dx.doi.org/10.1021/acsanm.0c02886
ACS Appl. Nano Mater. 2021, 4, 580−589

phase,[15] so the nitrogen-containing half of the nanotube was functionalized with PS.

Fracture toughness for the polymer interface without nanotubes was found to average 1.56 J/m^2 about half of that published elsewhere.[46] Control experiments with nanotubes without block polymerization increased the fracture toughness to around 5 J/m^2. The pristine nanotubes should reside within the PMMA phase of a polymer blend; however, with no mechanical energy to force them away from the interface, some likely remain where originally placed. With block-polymerized nanotubes, the strength was found to be further increased to an average of 23.3 J/m^2, which is 15 times stronger than the bare interface and 4.6 times stronger than regular nanotubes. The increase of 22 J/m^2 is similar to the increase in the literature shown for block copolymers at the interface.[46] It should be noted that some nanotube aggregates are present in the nanotube suspensions used during the spin coating process. This creates a nonuniform layer of nanotubes at the polymer−polymer interface. Due to this as well as the fact that much of the solution is lost during the spin coating process, the amount of nanotubes introduced via spin coating suspension divided by the surface area of the polymer interface is reported rather than a thickness at the interface. Nevertheless, these proof-of-concept experiments show that improvement took place at a level comparable to block−copolymer addition. We recognize that this improvement is a lower limit of what could be achieved with much improved interfacial strength measurements expected with improved nanotube dispersion in the spin coating solution.

While many more questions must be answered before a direct comparison of this approach with block copolymers can be made, these preliminary results are quite promising. Future areas to address to further increase the potential practical impact include improving nanotube dispersions, such as through avoiding full removal of the solvent prior to spin coating similar to the approach used between the purification and functionalization stages or employing freeze-drying measures. In addition, as with many applications of carbon nanotubes, efforts to further minimize purification costs are important to fully realize the potential of this approach when compared with the traditional use of block copolymers. More work needs to be done to optimize the nanotube/surface area ratio, nanotube dispersion technique, and the annealing time to potentially further increase the strengthening effect from the BF-CNTs, but we believe these results show that this technique has great promise.

CONCLUSIONS

In summary, carbon nanotubes with nitrogen incorporated with a concentration gradient along the length of the nanotube have been grown on vermiculite and purified to over 95 wt %. The nanotubes were functionalized with polystyrene by NMRP using TEMPO as a mediator. Polymer growth was selective to the nitrogen-containing half of the nanotube, as the pyridinic nitrogen sites mediate the strong radical scavenging properties of CNTs enabling the initialization of the NMRP. These block-polymerized nanotubes were placed at a PS/PMMA interface, and the fracture toughness of the interface was tested with the ADCB method. The block nanotubes significantly increased the fracture toughness showing an important use of these nanotubes for the stabilization of immiscible polymer blends.

METHODS

Nanotube Growth and Purification. All chemicals were purchased from Sigma-Aldrich and were of ACS reagent grade >98% or higher; all gases were from Airgas and were UHP or in the case of air zero grade. Vermiculite (Sigma-Aldrich product Z765422) was homogenized in water and wet-sieved to 150−350 μm in size. The catalyst precursor was 40 wt % iron (III) nitrate nonahydrate (Sigma-Aldrich product 216828), 15 wt % cobalt[22] nitrate hexahydrate (Sigma-Aldrich product 239267), and 45 wt % aluminum nitrate nonahydrate (Sigma-Aldrich product 237973) in a 1 molar solution. The catalyst solution was impregnated into the vermiculite via incipient wetness, followed by calcination at 450 °C. The incipient wetness impregnation was repeated a total of three times to ensure maximum coverage.

Five grams of the final catalyst + support was placed in a 1″ quartz tube above a quartz frit. Hydrogen was allowed to flow through the reactor at 300 sccm as the reactor was heated to 650 °C at 10 °C/min. The reactor was held at 650 °C to ensure complete reduction of the catalyst. The gas was switched to 300 sccm of argon as the reactor was heated to a growth temperature of 725 °C. At the growth temperature, the fluidized bed height is approximately 10″. Acetonitrile (Sigma-Aldrich product 271004) was injected into the reactor at 80 °C for 2.5 min at 300 mL/h to grow the nitrogen-containing portion of the nanotube while argon flow was continued to maintain fluidization of the bed. After the acetonitrile was stopped, the reactor was given 30 s to purge before ethylene flow was started at 200 sccm for 1 min to accomplish the pristine portion of the growth. The reactor was cooled to room temperature under a constant argon flow.

The vermiculite support was removed via sequential base−acid reactions. Anhydrous sodium hydroxide (Sigma-Aldrich product 795429) was heated to 400 °C in a single-use steel container. The nanotubes on the substrate were stirred into the molten NaOH until dissolved, yielding a water-soluble sodium silicate, free CNTs, and magnesium oxide. The mixture was cooled to room temperature and dissolved in water. The solution was slowly titrated with 0.1 M HCl to change the now magnesium hydroxide to water-soluble $MgCl_2$. The resulting solution was filtered and washed with water until the runoff pH was neutral. Nanotubes destined for functionalization were never fully dried, which would cause severe entanglement of the nanotubes.

During filtration shortly before the water wash was finished, the wash was switched to acetone for 100 mL. After acetone, the wash was switched to benzene, again for 100 mL. At no point were two separate phases observed. The final result of the purification and wash was nanotubes suspended in and stored in benzene until functionalization to prevent agglomeration. The nanotube product when dry was 90% CNT, 5% amorphous carbon, and 5% residual as measured by TGA in air, shown in Figure 2a.

Nanotube Functionalization. One gram of the nanotubes suspended in 100 mL of benzene was reacted with 0.1 g of benzoyl peroxide (Sigma-Aldrich product 179981) for 1 h at reflux temperature, followed by reaction with a 1:1.3 molar ratio of BPO to TEMPO (Sigma-Aldrich product 214000) for 1 h, filtered, and lightly washed in benzene. The nanotubes were then suspended in 300 mL of benzene and 200 mL of styrene (Sigma-Aldrich product S4972). The reactor was heated to 80 °C and allowed to polymerize for 24 h. The polymerized nanotubes were washed three times in benzene to remove unattached polymer.

Asymmetrical Double Cantilever Beam Test. PS (average MW = 192 000) and PMMA (average MW = 120 000) were compression-molded into sheets 6cm × 5cm and thicknesses of 2.4 and 2.0 mm, respectively. One milligram of dried nanotubes was dispersed in toluene via bath sonication for 20 min and then spin-coated on a PMMA wafer. It should be noted that the majority of the nanotube solution is lost during the spin coating process, so while the amount of nanotube dispersion coated on the surface is reported, the exact amount of nanotubes left on the surface is not quantified. We recognize that some nanotube breakage may occur with this treatment, which means that the interfacial reinforcement measured

https://dx.doi.org/10.1021/acsanm.0c02886
ACS Appl. Nano Mater. 2021, 4, 580−589

is likely an underestimation of what is possible with block nanotubes without drying and redispersion. Once the toluene evaporated, a PS wafer was joined to the previously coated PMMA wafer in a compression molder at 120 °C for 6 h. The specimen was cut into 6 cm × 8 mm pieces before testing. A razor blade was inserted at the interface between the two beams using a servo motor at a constant speed. Once the crack propagated, a picture is taken, and the length of the crack is measured using Image J. That length is used to calculate the fracture toughness based on the elastic foundation model proposed by Kramer.[47]

TGA-MS. Temperature-programmed desorption (TPD) of purified CN_xNTs was performed on a Netzsch STA 449F1 equipped with a pin thermocouple and a Netzsch nanobalance. Outlet gases were analyzed by mass spectroscopy on an Aeolos QMS. Temperature-programmed adsorption (TPA) measurements were carried out under argon with a ramp rate of 2 °C/min, and H_2O, CO, NO, CO_2, and NO_2 levels were monitored. Of the expected oxygenated species, only CO_2 was observed as being thermally evolved in the range of 300−450 °C. The entirety of the mass loss in this range was then recognized to be 32/44th oxygen for the oxygen concentration.

Temperature-programmed oxidation (TPO) of the CN_xNT sample was done again with a ramp rate of 2 °C/min to determine the nitrogen concentration. In this instance, both NO and N_2O can be seen coming off in addition to CO_2. Comparing the mass spectrum peak area to known samples for the NO and N_2O, the sample is found to be 0.68 wt % nitrogen. While this is below the nitrogen content of the Terrones' group nanotubes, the ratio of N/O is 40% higher in the case of our nanotubes, indicating that the polymerization that occurs should still be as a result of the nitrogen functionalities.

Electron Microscopy of BF-CNTs at Interface. Polymer blends were created by solution-casting a PS/PMMA/CNT solution in tetrahydrofuran (THF) onto lacey carbon TEM grids. The solution was created by dissolving 0.2 g of PMMA and 0.8 g of PS in 40 mL of THF. The solution was then sonicated until the polymer dissolved, at which point 0.1 g of the BF-CNTs was added to the solution and sonicated for 1 min to disperse. The solution was allowed to settle for 1 h so that nanotube agglomerates would fall out of solution. Two microliters of solution was placed on the grid, which was then annealed for 4 h at 120°C, which is above the glass-transition temperature. TEM was then carried out on a Zeiss 10 A at 60 keV. SEM was carried out for all steps on a Zeiss Neon operating at 1 keV with an in lense backscatter detector. Cross-sectional images were carried out by first using a table saw to cut a cross section (∼1 mm wide) of an ADCB sample containing the interface. The sample was then microtomed into 690 nm thin slices using a glass knife and imaged using a JEOL 2010F field emission transmission electron microscope.

XPS Analysis. X-ray photoelectron spectroscopy (XPS) analysis of the materials was performed with a PHI 5800 ESCA (Physical Electronics) system equipped with a standard Al Kα X-ray source (1486.6 eV) operating at 300 W (15 kV and 20 mA) and a concentric hemispherical analyzer. The materials were pretreated at 120 °C for 10 h in a flow of nitrogen (100 mL/min flow) prior to XPS analysis. An O-ring-sealed sample transfer vessel (PHI Model 04-110) was used to transfer the ex situ pretreated samples from the glovebag to the XPS chamber without atmospheric exposure. The samples were mounted on sample stubs using a double-sided conductive carbon tape. Survey spectra (0−1400 eV) were collected with a pass energy of 187.85 eV. The high-resolution XPS spectra of C 1s and N 1s were measured using a pass energy of 23.50 eV. All data were collected at a 45° takeoff angle. The binding energy values were referenced to the adventitious hydrocarbon C 1s peak at 284.8 eV. The core-level peaks were analyzed by PHI MultiPak (Version 9.5).

■ ASSOCIATED CONTENT

Supporting Information

The Supporting Information is available free of charge at https://pubs.acs.org/doi/10.1021/acsanm.0c02886.

TEM image of PS-functionalized nanotube repulsive interaction via insertion into the PMMA phase (Figure S1); and additional XPS elemental information and full width at half-maximum experimental information (Tables S1 and S2) (PDF)

■ AUTHOR INFORMATION

Corresponding Author

Steven Crossley − *School of Chemical, Biological, and Materials Engineering, University of Oklahoma, Norman, Oklahoma 73069, United States;* orcid.org/0000-0002-1017-9839; Email: stevencrossley@ou.edu

Authors

Lawrence Barrett − *School of Chemical, Biological, and Materials Engineering, University of Oklahoma, Norman, Oklahoma 73069, United States*

Fatoumata Ide Seyni − *School of Chemical, Biological, and Materials Engineering, University of Oklahoma, Norman, Oklahoma 73069, United States*

Mallikharjuna Rao Komarneni − *School of Chemical, Biological, and Materials Engineering, University of Oklahoma, Norman, Oklahoma 73069, United States*

John A. Zapata-Hincapie − *School of Chemical, Biological, and Materials Engineering, University of Oklahoma, Norman, Oklahoma 73069, United States*

Daniel T. Glatzhofer − *Department of Chemistry and Biochemistry, University of Oklahoma, Norman, Oklahoma 73069, United States*

Brian P. Grady − *School of Chemical, Biological, and Materials Engineering, University of Oklahoma, Norman, Oklahoma 73069, United States;* orcid.org/0000-0002-4975-8029

Complete contact information is available at: https://pubs.acs.org/10.1021/acsanm.0c02886

Author Contributions

The manuscript was written through contributions of all authors. S.C. and B.P.G. conceived the idea. L.B. carried out block nanotube synthesis, purification, selective functionalization, and all TGA runs and SEM images and non-ADCB TEM images. F.I.S. carried out the fracture toughness measurements and ADCB TEM images. M.R.K. carried out the XPS experiments. J.A.Z.-H. helpfully participated in discussions. D.T.G. helped advise functionalization approaches and proposed possible mechanisms. All authors have given approval to the final version of the manuscript.

Funding

The authors gratefully acknowledge support for this work from NSF award 1436532 and NSF CAREER award 1653935. Support from NSF grant 2022297 is also gratefully acknowledged for the TEM images at the interface of ADCB samples.

Notes

The authors declare no competing financial interest.

■ ACKNOWLEDGMENTS

The authors would like to thank Preston Larson and Julian Sabisch for their helpful assistance with the electron microscope imaging.

■ ABBREVIATIONS

CNT, carbon nanotube

PS, polystyrene
PMMA, poly(methyl methacrylate)

REFERENCES

(1) *Plastics: Material-Specific Data*; EPA, 2015.
(2) Thomas, S.; Prud, R. E. Compatibilizing effects of block copolymers in heterogeneous polystyrene/poly(methylmethacrylate) blends. *Polymer* **1992**, *33*, 4260−4268.
(3) Macosko, C. W.; Guegan, P.; Khandpur, A. K.; Nakayama, A.; Marechal, P.; Inoue, T. Compatibilizers for Melt Blending: Premade Block Copolymers. *Macromolecules* **1996**, *29*, 5590−5598.
(4) Brown, H. R.; Char, K.; Deline, V. R.; Green, P. F. Effects of Diblock Copolymer on Adhesion between Immersible Polymers. 1. PS-PMMA Copolymer between PS and PMMA. *Macromolecules* **1993**, *26*, 4155−4163.
(5) Mori, Y.; Lim, L. S.; Bates, F. S. Consequences of molecular bridging in lamellae-forming triblock/pentablock copolymer blends. *Macromolecules* **2003**, *36*, 9879−9888.
(6) Vigild, M. E.; Chu, C.; Sugiyama, M.; Chaffin, K. A.; Bates, F. S. Influence of shear on the alignment of a lammelae-forming pentablock copolymer. *Macromolecules* **2001**, *34*, 951−964.
(7) Gegenhuber, T.; Krekhova, M.; Schöel, J.; Gröschel, A.; Schmalz, H. Patchy Carbon Nanotubes as Efficient Compatibilitiy for Polymer Blends. *ACS Macro Lett.* **2016**, *5*, 306−310.
(8) Gegenhuber, T.; Groschel, A.; Lobling, T.; Drechsler, M.; Ehlert, S.; Forester, S.; Schmalz, H. Noncovalent Grafting of Carbon Nanotubes with Triblock Terpolymers: Toward Patchy 1D Hybrids. *Macromolecules* **2015**, *48*, 1767−1776.
(9) Wei, C.; Cho, K.; Srivastava, D. Tensile strength of carbon nanotubes under realistic temperature and strain rate. *Phys. Rev. B* **2003**, *67*, No. 115407.
(10) Yu, M.-F.; Lourie, O.; Dyer, M.; Moloni, K.; Kelly, T.; Rouff, R. Strength and Breaking Mechanism of Multiwalled Carbon Nanotubes Under Tensile Load. *Science* **2000**, *287*, 637−640.
(11) Ruoff, R. S.; Tersoff, J.; Lorents, D.; Subramoney, S.; Chan, B. Radial Deformation of Carbon Nanotubes by van der Waals forces. *Nature* **1993**, *364*, 514−516.
(12) Palaci, I.; Fedrigo, S.; Brune, H.; Klinke, C.; Chen, M.; Riedo, E. Radial Elasticity of Multiwalled Carbon Nanotubes. *Phys. Rev. Lett.* **2005**, *94*, No. 175502.
(13) Minary-Jolandan, M.; Yu, M.-F. Reversible radial deformation up to the complete flattening of carbon nanotubes in nano-indentation. *J. Appl. Phys.* **2008**, *103*, No. 073516.
(14) Zhao, X.; Wang, H.; Fu, Z.; Li, Y. Enhanced interfacial adhesion by reactive carbon nanotubes: new route to high-performance immiscible polymer blend nanocomposites with simultaneously enhanced toughness, tensile strength, and electrical conductivity. *ACS Appl. Mater. Interfaces* **2018**, *10*, 8411−8416.
(15) Guo, J.; Briggs, N.; Crossley, S.; Grady, B. P. Morphology of Polystyrene/Poly(methyl methacrylate) Blends: Effects of Carbon Nanotubes Aspect Ratio and Surface Modification. *AIChE J.* **2015**, *61*, 3500−3510.
(16) Du, B.; Handge, U. A.; Majeed, S.; Abetz, V. Localization of functionalized MWCNT in SAN/PPE blends and their influence on rheological properties. *Polymer* **2012**, *53*, 5491−5501.
(17) Gültner, M.; Goldel, A.; Potschke, P. Tuning the localization of functionalized MWCNTs in SAN/PC blends by reactive component. *Compos. Sci. Technol.* **2011**, *72*, 41−48.
(18) Nayak, G. C.; Sahoo, S.; Rajasekar, R.; Das, C. K. Novel Approach for the selective dispersion of MWCNTs in the nylon/San blend system. *Composites, Part A* **2012**, *43*, 1242−1251.
(19) Tao, F.; Nysten, B.; Baudouin, A.-C.; Thomassin, J.-M.; Vuluga, D.; Detrembleur, C.; Bailly, C. Influence of nanoparticle-polymer interactions on the apparent migration behavior of carbon nanotubes in an immiscible polymer blend. *Polymer* **2011**, *52*, 4798−4805.
(20) Qu, L.; Dai, L.; Osawa, E. Shape/Size-Controlled Syntheses of Metal Nanoparticles for Site-Selective Modification of Carbon Nanotubes. *J. Am. Chem. Soc.* **2006**, *128*, 5523−5532.
(21) Wei, C.; Dai, L.; Roy, A.; Tolle, T. B. Multifunctional Chemical Vapor Sensors of Aligned Carbon Nanotube and Polymer Composites. *J. Am. Chem. Soc.* **2006**, *128*, 1412−1413.
(22) Wei, Z.; Kondratenko, M.; Dao, L. H.; Perepichka, D. F. Rectifying Diodes from Asymmetrically Functionalized Single-Wall Carbon Nanotubes. *J. Am. Chem. Soc.* **2006**, *128*, 3134−3135.
(23) Qu, L.; Dai, L. Polymer-masking for controlled functionalization of carbon nanotubes. *Chem. Commun.* **2007**, *297*, 3859−3861.
(24) Lee, K. M.; Li, L.; Dai, L. Asymmetric End-Functionalization of Multi-Walled Carbon Nanotubes. *J. Am. Chem. Soc.* **2005**, *127*, 4122−4123.
(25) Grady, B. P. *Carbon Nanotube−Polymer Composites: Manufacture, Properties, and Applications*; Wiley, 2011.
(26) Datsyuk, V.; Kalyva, M.; Papagelis, K.; Parthenios, J.; Tasis, D.; Siokou, A.; Kallitsis, I.; Galiotis, C. Chemical Oxidation of Multiwalled Carbon Nanotubes. *Carbon* **2008**, *46*, 833−840.
(27) Bulusheva, L. G.; Okotrub, A. V.; Fedoseeva, Y. V.; Kurenya, A. G.; Asanoc, I. P.; Vilkov, O. Y.; Koos, A. A.; Grobert, N. Controlling pyridinic, pyrrolic, graphitic, and molecular nitrogen in multi-wall carbon nanotubes using precursors with different N/C ratios in aerosol assisted chemical vapor deposition. *Phys. Chem. Chem. Phys.* **2015**, *17*, 23741−23747.
(28) Koós, A. A.; Dowling, M.; Jurkschat, K.; Crossley, A.; Grobert, N. Effect of the experimental parameters on the structure of nitrogen doped carbon nanotubes produced by aerosol chemical vapour deposition. *Carbon* **2009**, *47*, 30−37.
(29) Nevidomskyy, A. H.; Csányi, G.; Payne, M. C. Chemically Active Substitutional Nitrogen Impurity in Carbon Nanotubes. *Phys. Rev. Lett.* **2003**, *91*, No. 105502.
(30) Arrigo, R.; Havecker, M.; Schlogl, R.; Su, D. S. Dynamic surface rearrangement and thermal stability of nitrogen functional groups on carbon nanotubes. *Chem. Commun.* **2008**, 4891−4893.
(31) Wang, B.; Tsetseris, L.; Pantelides, S. T. Introduction of nitrogen with controllable configuration into graphene via vacancies and edges. *J. Mater. Chem. A* **2013**, *1*, 14927−14934.
(32) Valaskova, M.; Martynkova, G. S. Vermiculite: Structural Properties and Examples of the Use. In *Clay Minerals in Nature—Their Characterization, Modification and Application*; IntechOpen: London, 2012; pp 211−238.
(33) Essington, M. E. *Soil and Water Chemistry: An Integrative Approach*, 2nd ed.; CRC Press, 2015.
(34) Kalinowski, B. E.; Schweda, P. Rates and nonstoichiometry of vermiculite dissolution at 22°C. *Geoderma* **2007**, *142*, 197−209.
(35) Raymundo-Piñero, E.; Azais, P.; Cacciaguerra, T.; Cazorla-Amoros, D.; Linares-Solano, A.; Beguin, F. KOH and NaOH activation mechanism of multiwalled carbon nanotubes with different structural organisation. *Carbon* **2005**, *43*, 786−795.
(36) Bulusheva, L.; Okotrub, A.; Fedoseeva, Y. V.; Kurenya, A.; Asanov, I.; Vilkov, O.; Koós, A. A.; Grobert, N. Controlling pyridinic, pyrrolic, graphitic, and molecular nitrogen in multi-wall carbon nanotubes using precursors with different N/C ratios in aerosol assisted chemical vapor deposition. *Phys. Chem. Chem. Phys.* **2015**, *17*, 23741−23747.
(37) Dehonor, M.; Masenelli-Varlot, K.; Gonzalez-Montiel, A.; Gauthier, C.; Caville, J. Y.; Terrones, H.; Terrones, M. Nanotube brushes: polystyrene grafted covalently on CNx nanotubes by nitroxide-mediated radical polymerization. *Chem. Commun.* **2005**, 5349−5351.
(38) O'Hara, F.; Blackmond, D. G.; Baran, P. S. Radical-based regioselective C−H functionalization of electron-deficient heteroarenes: scope, tunability, and predictability. *J. Am. Chem. Soc.* **2013**, *135*, 12122−12134.
(39) Paquette, L. A.; Breslow, R. *Principles of Modern Heterocyclic Chemistry*; Benjamin: New York, 1968.
(40) Fan, D.-Q.; He, J.-P.; Tang, W.; Xu, J.-T.; Yang, Y.-L. Synthesis of polymer grafted carbon nanotubes by nitroxide mediated radical polymerization in the presence of spin-labeled carbon nanotubes. *Eur. Polym. J.* **2007**, *43*, 26−34.

https://dx.doi.org/10.1021/acsanm.0c02886
ACS Appl. Nano Mater. 2021, 4, 580−589

(41) Zhao, X.-D.; Fan, X.-H.; Chen, X.-F.; Chai, C.-P.; Zhou, Q.-F. Surface Modification of Multiwalled Carbon Nanotubes via Nitroxide-Mediated Radical Polymerization. *J. Polym. Sci., Part A: Polym. Chem.* **2006**, *44*, 4656−4667.
(42) Dintcheva, N.; Arrigo, R.; Teresi, R.; Megna, B.; Gambarotti, C.; Marulllo, S.; D'Anna, F. Tunable radical scavenging activity of carbon nanotubes through sonication. *Carbon* **2016**, *107*, 240−247.
(43) Shi, X.; Jiang, B.; Wang, J.; Yang, Y. Influence of wall number and surface functionalization of carbon nanotubes on their antioxidant behavior in high density polyethylene. *Carbon* **2012**, *50*, 1005−1013.
(44) Biddinger, E. J.; Von Deak, D.; Ozkan, U. S. Nitrogen-containing carbon nanostructures as oxygen-reduction catalysts. *Top. Catal.* **2009**, *52*, 1566−1574.
(45) Creton, C.; Kramer, E.; Hui, C.-Y.; Brown, H. Failure mechanisms of polymer interfaces reinforced with block copolymers. *Macromolecules* **1992**, *25*, 3075−3088.
(46) Bernard, B.; Brown, H.; Hawker, C.; Kellock, A.; Russell, T. Adhesion of Polymer Interfaces Reinforced with Random and Diblock Copolymers as a Function of Geometry. *Macromolecules* **1999**, *32*, 6254−6260.
(47) Xiao, F.; Hui, C.-Y.; Kramer, E. Analysis of a mixed mode fracture specimen: the asymmetric double cantilever beam. *J. Mater. Sci.* **1993**, *28*, 5620−5629.

https://dx.doi.org/10.1021/acsanm.0c02886
ACS Appl. Nano Mater. 2021, 4, 580−589